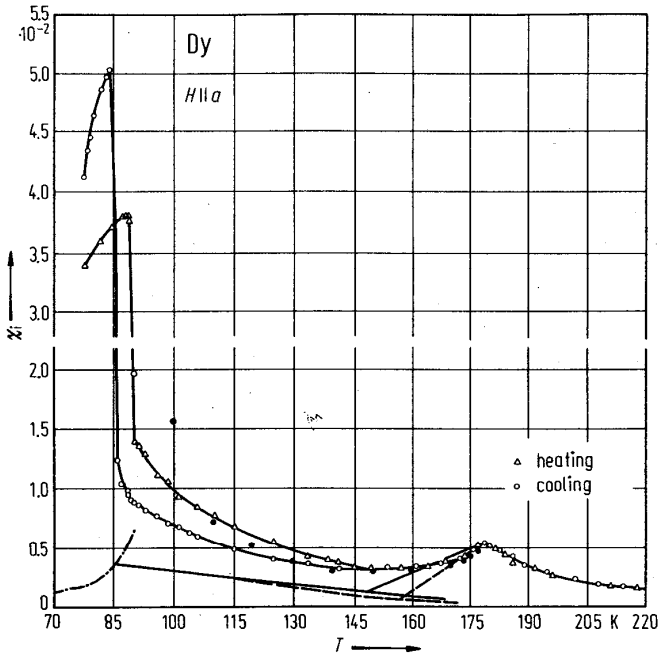

Fig. 243. Dy. Initial magnetic volume susceptibility, χ_i, in SI units, along the a axis in Dy deduced on heating (triangles) and cooling (open circles) from χ_{ac} (21 Hz) measurements at $H=0$ [74 M 3], and (solid circles) from the initial slope of the magnetization curves [58 B 1]. The strong temperature hysteresis of $\cong 5$ K and the discontinuous change of χ_i at $T_C=85$ K may be connected with the existence of antiferromagnetic domains in which the ferromagnetically coupled layers spiral uniformly but in opposite sense. The solid and dashed lines are calculated assuming that, in the helical phase, the Fourier-transformed exchange integral at the modulation wavevector, $J(Q)$, scales as m^2, $J(Q) \propto m^2$, and m, $J(Q) \propto m$, respectively, where m is the reduced Dy magnetic moment. The dashed-dotted line in the ferromagnetic phase represents χ_i calculated for intrinsic domain wall pinning [74 M 3].

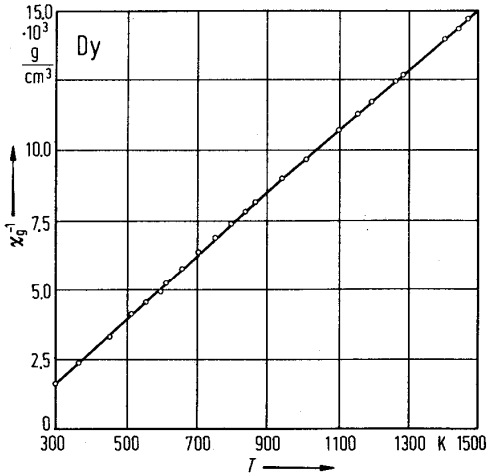

Fig. 248. Temperature dependence of reciprocal magnetic susceptibility for Dy in the higher-temperature range between 300 and 1500 K showing Curie-Weiss law with $p_{eff}=10.67\,\mu_B$/Dy and $\Theta=151(1)$ K [61 A 1].

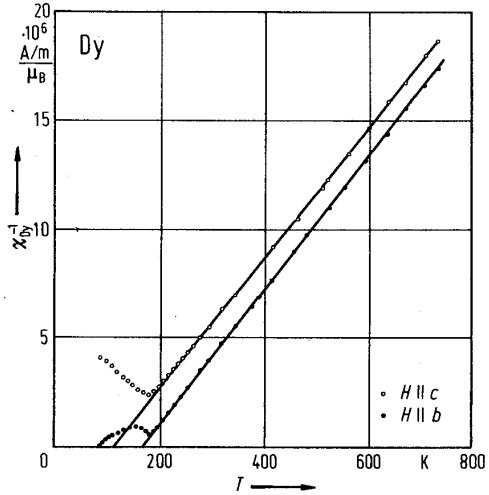

Fig. 249. Reciprocal initial magnetic susceptibility per atom for two main crystallographic axes of a Dy single crystal [77 T 1].

Fig. 244. Reciprocal magnetic volume susceptibility, in SI units, in the basal plane, χ_{ab}^{-1}, and along the c axis, χ_c^{-1}, in the helical and paramagnetic phases. The highest applied magnetic field in the helical phase was $0.64 \cdot 10^6$ Am^{-1} (8 kOe). In the paramagnetic phase the applied fields ranged from $0.4 \cdot 10^6$ Am^{-1} (5 kOe) to $2.8 \cdot 10^6$ Am^{-1} (35 kOe). The full curves are calculations including a mean-field model. The broken curve gives χ_c^{-1} for $d(B_2^0/\alpha_J)/d(c/a)=0.16 \cdot 10^4$ K, where B_2^0 is a CEF parameter and α_J is the 2nd-order Stevens factor [77 F 1].

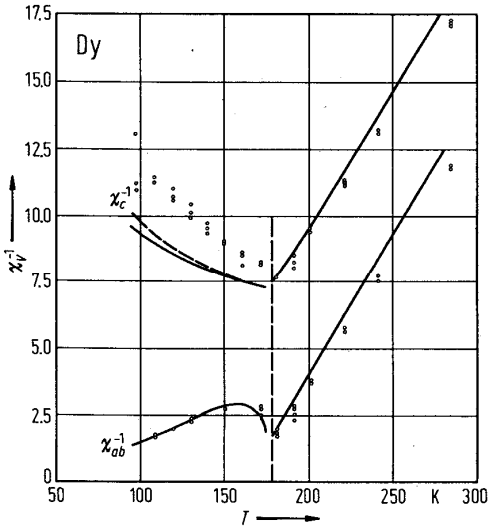

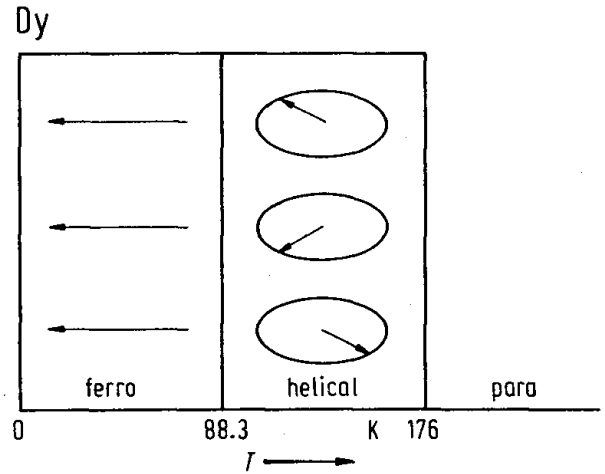

Fig. 232. Ordered spin structures observed by neutron diffraction for Dy [61 W 2].

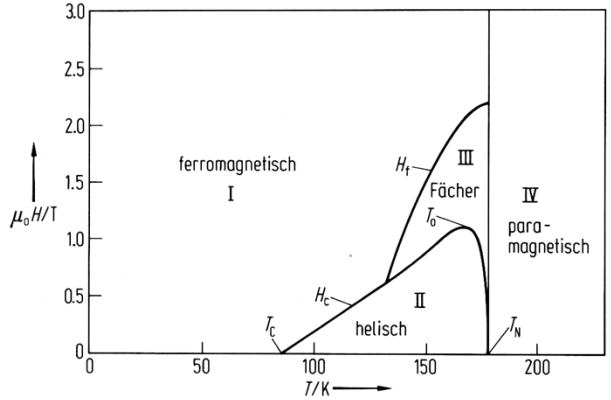

Abb. 8.22 Phasendiagramm der Spinstrukturen in Dysprosium in Abhängigkeit von der Temperatur und einem Magnetfeld, das parallel zur ⟨1120⟩-Richtung des hexagonalen Kristalls angelegt wurde [37].

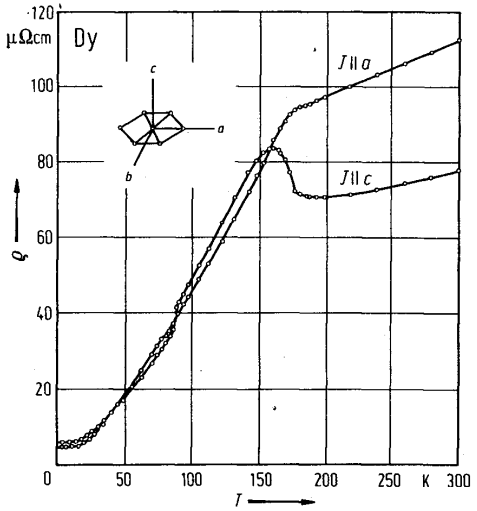

Fig. 278. Temperature variation of the electrical resistivities of Dy single crystal in the temperature range covered, 4.2···300 K, along the *a* and *c* axis. The ferromagnetic to helical transition gives a sudden increase of resistivity at 89 K in the *c* direction. At the Néel temperature, there is an anomalous behaviour, but more pronounce for the *c* direction [68 B 4].

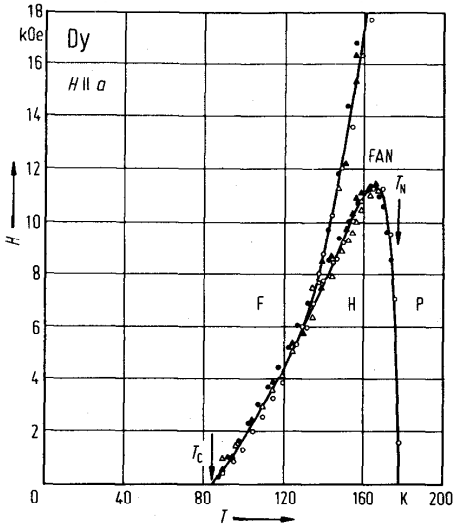

Fig. 279. Magnetic phase diagram giving the different magnetic ordering of Dy as function of the temperature, *T*, and the magnetic field, *H*, applied along the *a* direction, as deduced from transverse magnetoresistance data. P designates the paramagnetic phase, H the helical phase, F the ferromagnetic phase and FAN the intermediate fan phase; the boundary between the fan phase and the paramagnetic phase is not given here. The symbols used indicate data from three different single-crystal samples [73 A 1].

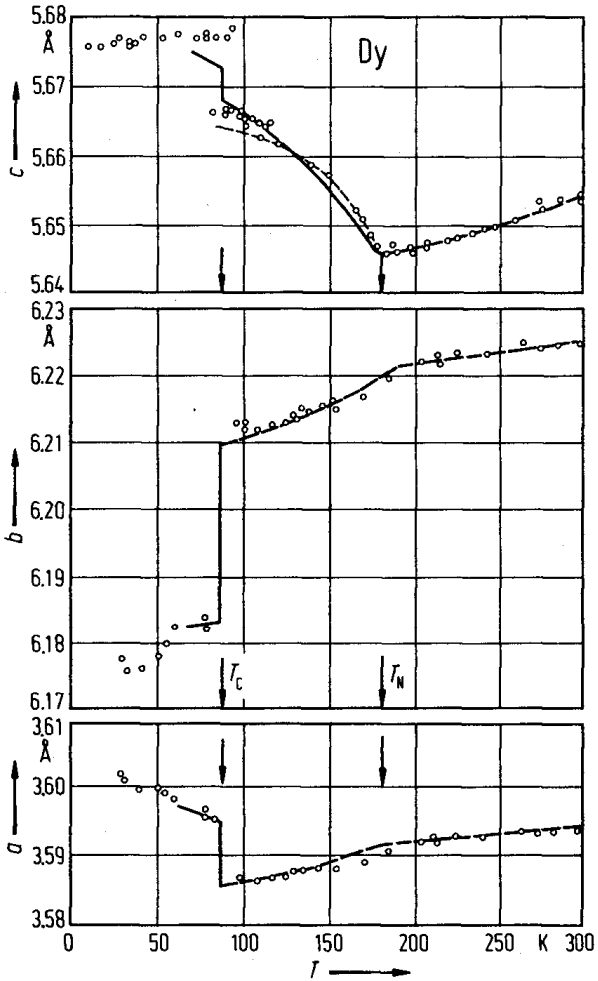

Fig. 275. ***a***, ***b***, ***c*** **axis lattice parameter as a function of temperature for Dy from X-ray studies [63 D 3]. The discontinuity in lattice constants for Dy at T_C corresponds to an orthorhombic distortion of the hcp lattice. Bulk strain gauge results are given for comparison by the dashed line in the range $T \geqq T_C$. The solid line shown for the *c* axis of Dy is a fit to the molecular field expression. The magnitude of the discontinuity is as calculated in [69 E 1].**

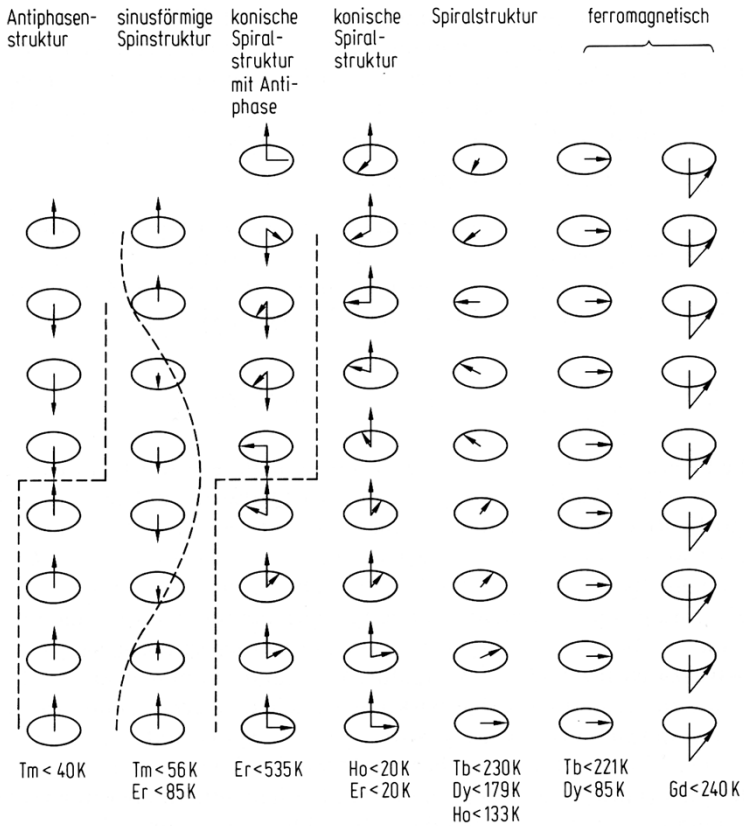

Abb. 8.21 Spinstrukturen der Seltenerdmetalle; aufgrund der fluktuierenden, weitreichenden indirekten Austauschkopplung können beim gleichen Metall je nach Temperatur verschiedenartige Spinstrukturen auftreten (nach Koehler [78]).

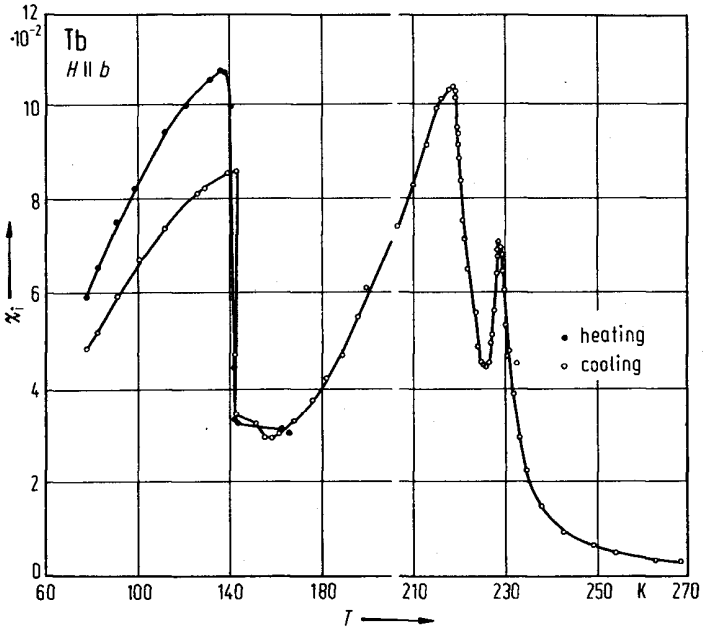

Fig. 191. Variation of the initial susceptibility, χ_i, in SI units of Tb measured along the *b* axis with temperature. χ_i represents the differential susceptibility deduced from χ_{ac} for $H=0$. Two high-temperature peaks are associated with magnetic phase transitions at $T_C=217.7$ and $T_N=228.5$ K. The peak at 135 K originates from a very large magnetic viscosity [74 M 3].

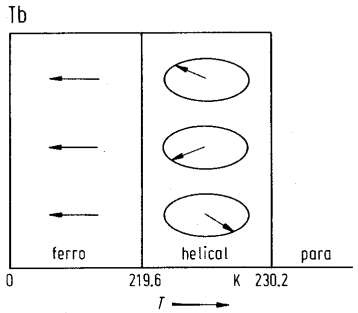

Fig. 174. Ordered spin structures observed by neutron diffraction for Tb [63 K 1].

Fig. 175. Helical turn angles as a function of temperature for Tb, showing the anomaly in the critical magnetic field at 223.1 K (open triangle) and $\omega=20°$ [83 G 1]. The broken line is an extrapolation of an approximately linear ω vs. T relation in the temperature range $216\,K<T<224\,K$ deduced from the neutron diffraction data (open circles) [67 D 1]. Arrows indicate T_N and T_C of [83 G 1] while the other T_N and T_C values are from work listed in [82 G 1].

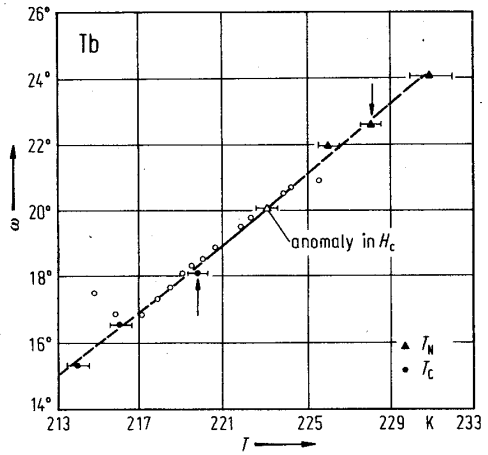

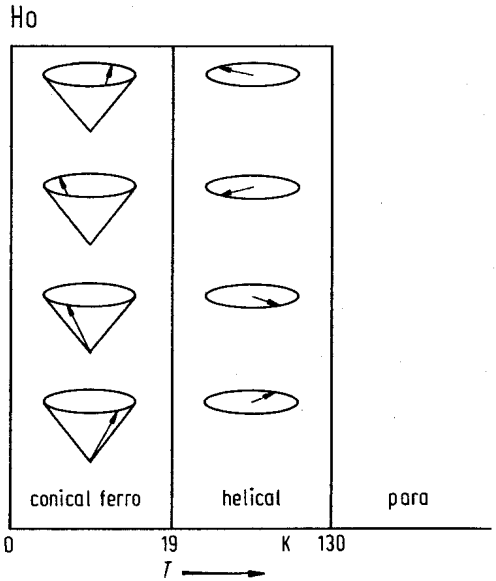

Fig. 295. Ordered spin structures observed by neutron diffraction for Ho [72 K 1].

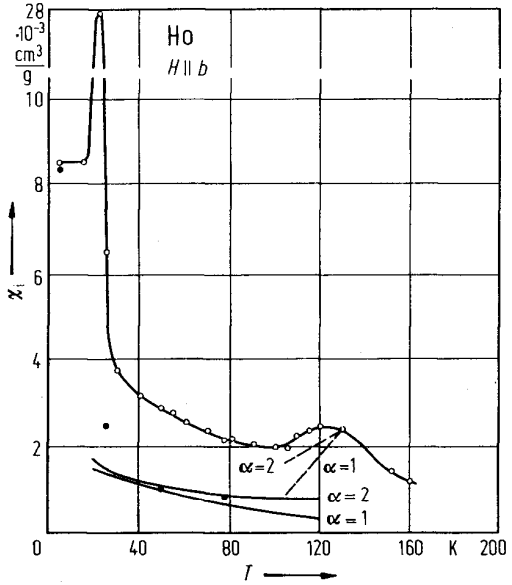

Fig. 309. Temperature dependence of the low-field magnetic susceptibility (open circles) of Ho taken from the initial slopes of the magnetization curves parallel to the *b* axis. The solid circles represent values calculated from the experimentally determined exchange integrals $J(q)$ in the helical and conical phases. Full and dashed lines represent calculations for, respectively, the helical phase and temperatures near T_N using exchange parameters determined experimentally at 78 K and scaled according to molecular field theory ($\alpha=2$) and random phase approximation ($\alpha=1$). The measured values are larger than the calculated values and this is tentatively ascribed to the presence of ferromagnetic domain walls separating spirals of opposite sense. The peaks at 20 and 130 K are associated with the helical⇌conical and paramagnetic⇌helical phase transitions, respectively [78 M 3].

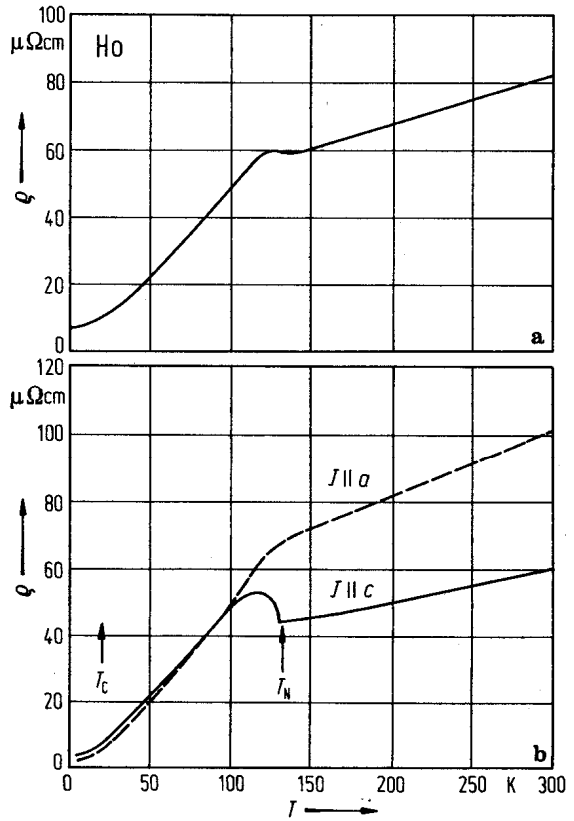

Fig. 327. Temperature dependence of the electrical resistivity, ϱ, of Ho for (a) polycrystals [60 C 2] and (b) a single crystal along the *a* and *c* axis [69 N 1].

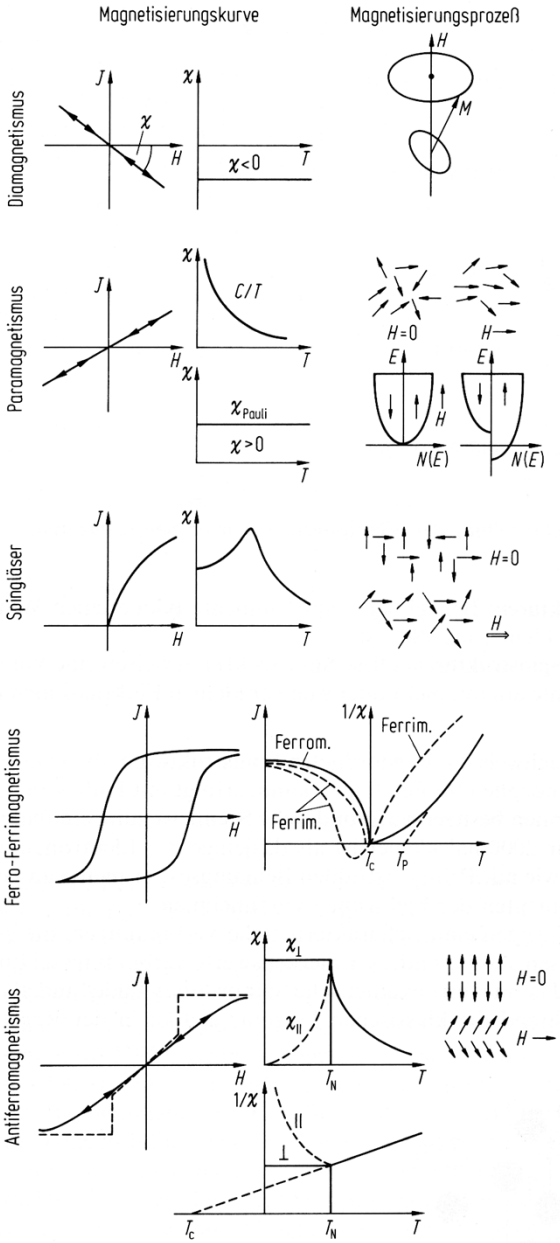

Abb. 8.3 Schematische Darstellung der Magnetisierungskurven, der Temperaturabhängigkeit der Suszeptibilität und der spontanen Magnetisierung verschiedener magnetischer Stoffe.